Journal Pre-proofs

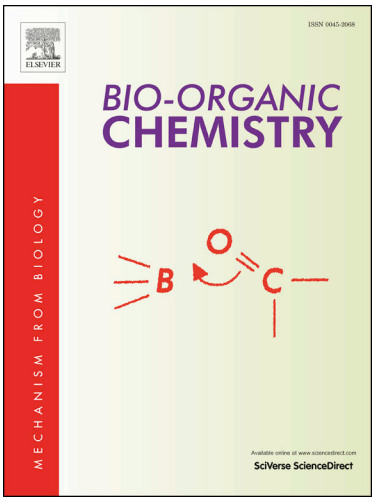

Diversity of complexes based on *p*-nitrobenzoylhydrazide, benzoylformic acid and diorganotin halides or oxides self-assemble: cytotoxicity, the induction of apoptosis in cancer cells and DNA-binding properties

Wujiu Jiang, Shanji Fan, Qian Zhou, Fuxing Zhang, Daizhi Kuang, Yuxing Tan

PII: S0045-2068(19)31049-1
DOI: https://doi.org/10.1016/j.bioorg.2019.103402
Reference: YBIOO 103402

To appear in: *Bioorganic Chemistry*

Received Date: 3 July 2019
Revised Date: 22 October 2019
Accepted Date: 24 October 2019

Please cite this article as: W. Jiang, S. Fan, Q. Zhou, F. Zhang, D. Kuang, Y. Tan, Diversity of complexes based on *p*-nitrobenzoylhydrazide, benzoylformic acid and diorganotin halides or oxides self-assemble: cytotoxicity, the induction of apoptosis in cancer cells and DNA-binding properties, *Bioorganic Chemistry* (2019), doi: https://doi.org/10.1016/j.bioorg.2019.103402

Diversity of complexes based on *p*-nitrobenzoylhydrazide, benzoylformic acid and diorganotin halides or oxides self-assemble: cytotoxicity, the induction of apoptosis in cancer cells and DNA-binding properties

Wujiu Jiang[a, *], Shanji Fan,[b] Qian Zhou,[c] Fuxing Zhang,[a] Daizhi Kuang[a] and Yuxing Tan[a, *]

a. Key Laboratory of Functional Metal-Organic Compounds of Hunan Province, Key Laboratory of Functional Organometallic Materials, University of Hunan Province, College of Chemistry and Materials Science, Hengyang Normal University, Hengyang 421008, PR China.

b. Department of Oncologysurgery, The First Affiliated Hospital of University South China, Hengyang 421001, PR China.

c. School of Basic Medical Sciences, Peking University Health Science Center, Beijing 100191, PR China.

* Email: jwj_china@163.com, tanyuxing@hynu.edu.cn

Abstract: Eight organotin(IV) complexes (**C1**-**C8**) have been synthesized and characterized by elemental analysis, fourier transform infrared spectroscopy (FT-IR), multinuclear nuclear magnetic resonance (^{1}H, ^{13}C and ^{119}Sn NMR), high resolution mass spectroscopy (HRMS) and single crystal X-ray structural analysis. Crystallographic data show that **C1** was a tetranuclear 16-membered macrocycle complex, **C2**-**C4** and **C7** were centrosymmetric dimer distannoxane and there was a Sn_2O_2 four-membered ring in the middle of the molecule, respectively, **C5** and **C6** are monoorganotin complexes due to the dehydroalkylation effect during the reaction, while **C8** forms a one-dimensional chain structure. The cytotoxicity of all complexes were tested by 3-(4,5)-dimethylthiahiazo(-z-y1)-3,5-di-phenytetrazoliumromide (MTT) assays against three human tumor cell lines NCI-H460, MCF-7 and HepG2. The dibutyltin complex **C2** has been shown to be more potent antitumor agents than other complexes and carboplatin. Cell apoptosis study of **C2** with

the high activity on HepG2 and MCF-7 cancer cell lines was investigated by flow cytometry, it was shown that the antitumor activity of **C2** was related to apoptosis, but it has different cell cycle arrest characteristics from platinum compounds, and the proliferation was inhibited by blocking cells in S phase. The DNA binding activity of the **C2** was studied by UV-visible absorption spectrometry, fluorescence competitive, viscosity measurements and gel electrophoresis, results shown **C2** can be well embedded in the double helix of DNA and cleave DNA.

Keywords: organotin complex; self-assemble; synthesis; crystal structure; apoptosis;

1 Introduction

Cisplatin as the first organometallic anticancer drug [1] was still used as a front-line wide-spectrum anticancer drug [2]. However, unbearable chemotherapy side-effects [3-8] and the emergence resistance [9-11] have limited the clinical effectiveness of cisplatin and related drugs. Screening new organometallic complexes with high anticancer activity, it was expected to overcome the defect of platinum-based chemotherapy agent and open a new way in organometallic anticancer drug treatment. Some complexes with high anticancer activity *in vitro* have been discovered, such as organotin complexes [12-15], ruthenium complexes [16, 17], gallium complexes [18, 19], metallocene complexes [20-23], etc. Research shows the structure of the diorganotin complexes were highly similar to cisplatin in the coordination mode, and most of them have better anticancer activity *in vitro* than cisplatin [24-26], so it was considered to be the promising alternative to platinum-based complexes as a new organometallic anticancer drug. Since Crowe [27] reported that diorganotin complexes have anticancer activity *in vitro*, many organotin complexes have been prepared, some of which have far superior anticancer activity to platinum-based complexes in breast cancer [28, 29], ovarian cancer [30], nasopharyngeal cancer [31, 32], colon cancer [33] and bladder cancer [34].

In addition, the activity of the diorganotin complex depends on multiple factors such as the type of hydrocarbon group, ligand type, molecular structure, etc. Because the diorganotin has a large lipid-water partition coefficient, we have designed a biocompatible nitrogen-containing hydrophilic multidentate ligand to regulate the lipid-water partition

coefficient of diorganotin and it can be used to regulate molecular structure types. In order to simplify the synthesis step, we have synthesized a series of organotin complexes by microwave-assisted one-pot self-assembly using the coordination ability of the ligand and organotin.

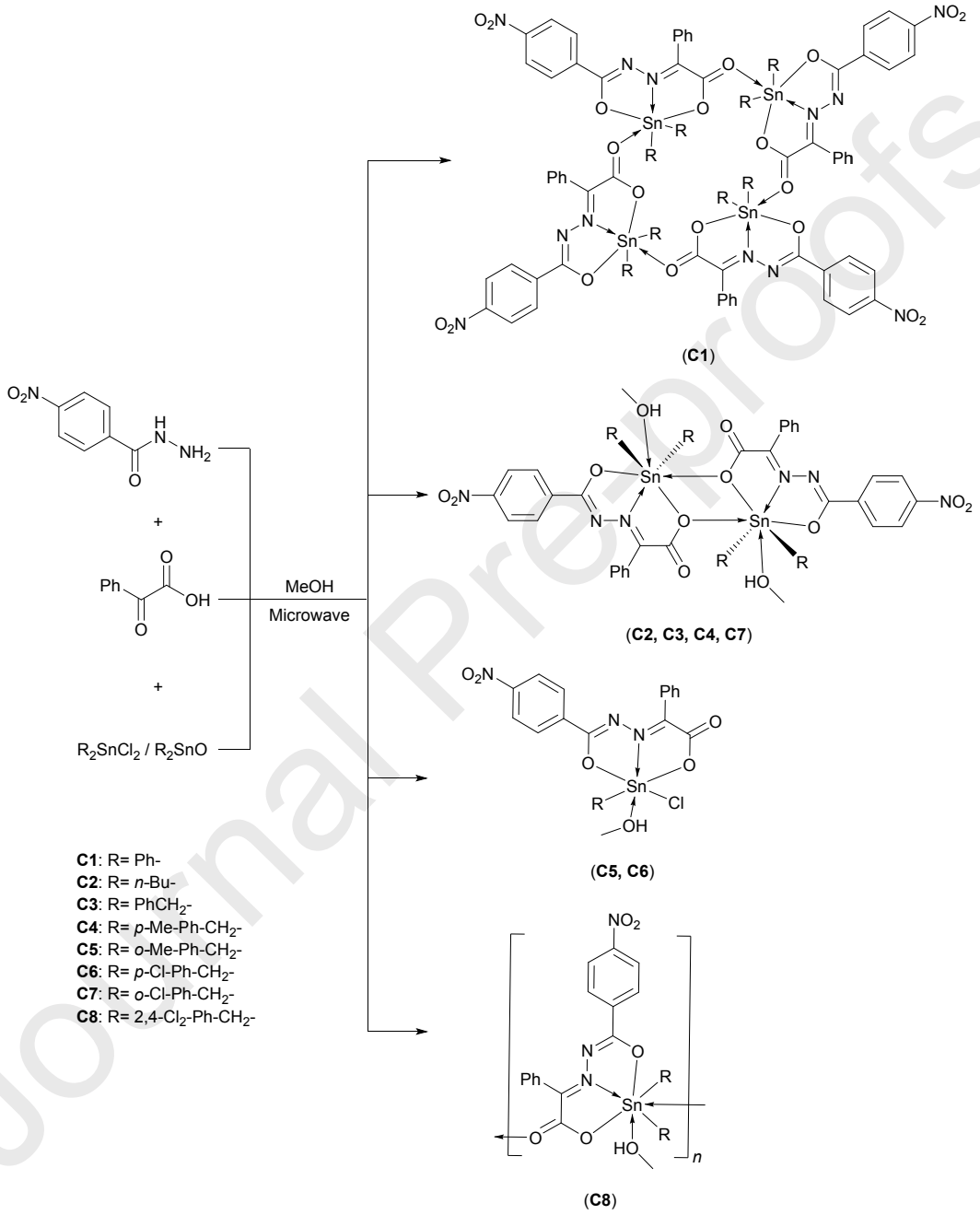

Scheme 1. The reactions of **C1-C8**.

In this paper, we report four types of organotin complexes, the cytotoxicity of these complexes against three human cancer cell lines (NCI-H460, MCF-7 and HepG2) was initially tested. HepG2 and MCF-7 cancer cell apoptosisinduced by **C2** was examined by flow

cytometry analysis, and the interaction mode of **C2** and DNA was studied by UV, fluorescence and viscosity, etc.

2 Experimental

2.1 Materials and methods

The microwave synthesis reaction was completed using Sineo Microwave MDS-10 High-throughput Microwave Sample Preparation Workstation. Elemental analyses for C, H, and N were determined on a PE-2400(II) analyzer. IR spectrum was obtained for KBr pellets on Shimadzu Prestige-21 spectrophotometer in the 4000-400 cm^{-1}. ^{1}H, ^{13}C and ^{119}Sn NMR analysis were performed on a Bruker AVANCE NMR spectrometer. HRMS was obtained by Thermo Scientific LTQ Orbitrap XL with ESI. Crystal structure was determined on a CCD area detector X-ray diffractometer. Thermogravimetric analyes (TGA) were recorded on a NETZSCH TG 209 F3 instrument at a heating rate of 20°C /min from room temperature to 900°C under air. Melting point measurement was executed on an X-4 binocular micromelting point apparatus with the temperature unadjusted. Cytotoxicity studies was test by Thermo Scientific Multiskan GO. UV-Vis absorption spectra was measured by UV-2550 spectrometer. Fluorescence spectra was obtained with a Hitachi F-7000 spectrophotometer with quartz cuvette (path length=1cm). Viscosity experiments were conducted on an Ubbelodhe viscometer. Gel electrophoresis was measured by DYY-6C Electrophoresis power supply. Cell apoptosis and cell cycle were measured by BD FACSCalibur CellSorting System.

Calf thymus DNA (Type XV, Activated, lyophilized powder) were from Sigma-Aldrich LLC., pBR322 DNA used in this study was synthesized by Sangon Biotech Co., Ltd. (Shanghai, China). 4-Nitrobenzhydrazide were from J&K Scientific Ltd. Dibutyltin oxide and benzoylformic acid were from TCI (Shanghai) Development Co., Ltd. Diphenyltin dichloride were from Alfa Aesar (China) Chemical Co., Ltd. Other chemicals were from Sinopharm Chemical Reagent Co., Ltd. All reagents were of analytical grade obtained from commercial sources and used without further purification. Ultrapure water (18.2 MΩ·cm) obtained from a Milli-Q water purification system (Millipore Co., USA) was used in all experiments. Tris-HCl ($0.01 mol \cdot L^{-1}$) buffer solution was prepared by a certain amount of Tris dissolved in super pure water before using, the pH of the solution

was adjusted to 7.40 with Hydrochloric acid solution (0.1 mol·L^{-1}). The purity of CT-DNA was determined by comparing the absorbance at 260 and 280 nm (A_{260}/A_{280}=1.8 ~ 1.9/1). The concentration of CT-DNA was calculated by measuring the absorbance at 260nm (ε_{260}=6600 L·mol^{-1}·cm^{-1}). The reserve solution is stored at 4°C. The ethidium bromide solution was prepared by a certain amount of ethidium bromide solid dissolved in Tris-HCl (0.01 mol·L^{-1}) buffer solution.

2.2 Synthesis

To a mixture of *p*-nitrobenzoylhydrazide (1 mmol), benzoylformic acid (1 mmol), the corresponding diorganotin halides or oxides (1 mmol) and methanol (30 mL) were added to the microware reaction kettle, and subjected to microwave treatment with 30 min at 100 °C. When the reaction kettle had cooled to room temperature, the solution in the kettle was filtered. The complexes crystals were obtained by controlling solvent evaporation.

{[*p*-NO_2-C_6H_4(O)C=N-N=C(Ph)COO](\(C_6H_5\))$_2$Sn}$_4$ (C1): Yellow crystals, Yield 81%. m.p.: 221-223°C. FT-IR (KBr, cm^{-1}): 3421, 3072, 3055, 2991, 1695, 1616, 1600, 1587, 1568, 1525, 1479, 1384, 1340, 1321, 1294, 1263, 1251, 1089, 1172, 1153, 1024, 1012, 871, 852, 815, 736, 712, 690, 592, 547, 449. ^{1}H NMR (500 MHz, $CDCl_3$, δ/ppm): 8.44 (d, *J* = 8.9 Hz, 2H), 8.34 (d, *J* = 8.9 Hz, 2H), 8.15-8.17 (m, 2H), 7.86-7.88 (m, 4H), 7.26-7.59 (m, 9H). ^{13}C NMR (126 MHz, $CDCl_3$, δ/ppm): 173.24, 162.53, 152.49, 150.28, 137.91, 136.11, 135.35, 132.47, 132.44, 131.71, 129.75, 129.60 ($^1J_{Sn-C}$ = 89.5 Hz), 127.99, 127.86, 123.65. ^{119}Sn NMR (187 MHz, $CDCl_3$, δ/ppm): -294.09. HRMS (ESI) m/z calcd for $C_{27}H_{20}N_3O_5Sn^+$ $[M+H]^+$ 586.0419 , found 586.0411.

{[*p*-NO_2-C_6H_4(O)C=N-N=C(Ph)COO](*n*-Bu_2)Sn(CH_3OH)}$_2$ (C2): Yellow crystals, Yield 76%. m.p.: 98-100°C (dec.). FT-IR (KBr, cm^{-1}): 3419, 3076, 3055, 2956, 2927, 2870, 2858, 1631, 1598, 1587, 1529, 1496, 1400, 1382, 1342, 1315, 1305, 1292, 1255, 1153, 1168, 1085, 1024, 1012, 869, 852, 821, 804, 731, 719, 707, 690, 630, 594, 574, 542, 410. ^{1}H NMR (500 MHz, $CDCl_3$, δ/ppm): 8.27-8.32 (m, 4H), 8.12-8.14 (m, 2H), 7.58-7.60 (m, 3H), 3.49 (s, 3H), 1.72-1.81 (m, 4H), 1.50-1.66 (m, 4H), 1.33-1.40 (m, 4H), 0.88 (t, *J* = 7.2 Hz, 6H). ^{13}C NMR (126 MHz, $CDCl_3$, δ/ppm): 173.51, 164.30, 151.89, 150.04, 138.38, 132.08, 131.90, 129.73, 128.61, 127.83, 123.47, 50.85, 26.86, 26.42, 23.35 ($^1J_{Sn-C}$ = 618.0

Hz), 13.51. ^{119}Sn NMR (187 MHz, $CDCl_3$, δ/ppm): -509.34. HRMS (ESI) m/z calcd for $C_{23}H_{28}N_3O_5Sn^+$ $[M\text{-}CH_3OH+H]^+$ 546.1045, found 546.1035.

{[*p*-NO_2-C_6H_4(O)C=N-N=C(Ph)COO]($C_6H_5CH_2$)$_2$Sn(CH_3OH)}$_2$ (C3): Yellow crystals, Yield 72%. m.p.: 102-104°C (dec.). FT-IR (KBr, cm^{-1}): 3568, 3080, 3057, 3024, 2943, 1643, 1632, 1597, 1582, 1524, 1493, 1383, 1346, 1302, 1244, 1171, 1155, 1088, 868, 854, 802, 760, 739, 718, 696, 631, 594, 552. 459. ^{1}H NMR (500 MHz, $CDCl_3$, δ/ppm): 8.25 (d, *J* = 8.5 Hz, 2H), 8.04 (d, *J* = 8.5 Hz, 2H), 7.47-7.55 (m, 3H), 7.37 (d, *J* = 7.5 Hz, 2H), 7.04 (d, *J* = 7.5 Hz, 4H), 6.93-6.97 (m, 6H), 3.53 (d, *J* = 11.6 Hz, $^2J_{Sn\text{-}H}$ = 128.4 Hz, 2H), 3.49 (s, 3H), 3.45 (d, *J* = 11.6 Hz, $^2J_{Sn\text{-}H}$ = 128.4 Hz, 2H). ^{13}C NMR (126 MHz, $CDCl_3$, δ/ppm): 173.48, 168.76, 149.88, 149.40, 138.75, 136.49, 131.13, 129.78, 128.97, 128.60, 128.49, 128.31, 127.46, 125.70, 123.34, 50.88, 36.91 ($^1J_{Sn\text{-}C}$ = 748.4 Hz). ^{119}Sn NMR (187 MHz, $CDCl_3$, δ/ppm): -637.87. HRMS (ESI) m/z calcd for $C_{29}H_{24}N_3O_5Sn^+$ $[M\text{-}CH_3OH+H]^+$ 614.0732, found 614.0725.

{[*p*-NO_2-C_6H_4(O)C=N-N=C(Ph)COO](*p*-Me-$C_6H_4CH_2$)$_2$Sn(CH_3OH)}$_2$ (C4): Yellow crystals, Yield 61%. m.p.:116-118°C (dec.). FT-IR (KBr, cm^{-1}): 3482, 3082, 3049, 2999, 2920, 1678, 1624, 1605, 1591, 1528, 1510, 1499, 1383, 1344, 1319, 1306, 1290, 1254, 1169, 1086, 1024, 870, 853, 814, 733, 710, 691, 631, 592, 546, 501, 461. ^{1}H NMR (500 MHz, $CDCl_3$, δ/ppm): 8.26 (d, *J* = 8.5 Hz, 2H), 8.05 (d, *J* = 8.5 Hz, 2H), 7.53 (t, *J* = 7.3 Hz, 1H), 7.47 (t, *J* = 7.3 Hz, 2H), 7.32-7.33 (m, 2H), 6.92 (d, *J* = 7.9 Hz, 4H), 6.77 (d, *J* = 7.9 Hz, 4H), 3.50 (s, 3H), 3.45 (d, *J* = 11.6 Hz, $^2J_{Sn\text{-}H}$ = 126.2 Hz, 2H), 3.39 (d, *J* = 11.6 Hz, $^2J_{Sn\text{-}H}$ = 126.2 Hz, 2H), 2.12 (s, 6H). ^{13}C NMR (126 MHz, $CDCl_3$, δ/ppm): 173.41, 168.31, 149.82, 149.57, 138.96, 135.24, 133.30, 131.10, 130.97, 129.76, 129.14, 128.45, 128.22, 127.34, 123.27, 50.88, 36.22 ($^1J_{Sn\text{-}C}$ = 748.9 Hz), 20.83. ^{119}Sn NMR (187 MHz, $CDCl_3$, δ/ppm): -638.91. HRMS (ESI) m/z calcd for $C_{31}H_{28}N_3O_5Sn^+$ $[M\text{-}CH_3OH+H]^+$ 642.1045, found 642.1036.

[*p*-NO_2-C_6H_4(O)C=N-N=C(Ph)COO](CH_3OH)(*o*-Me-$C_6H_4CH_2$)SnCl (C5): Light yellow crystals, Yield 41%. m.p.: 145-147°C (dec.). FT-IR (KBr, cm^{-1}): 3107, 3053, 3022, 2970, 1667, 1593, 1526, 1479, 1445, 1385, 1346, 1321, 1304, 1290, 1258, 1175, 1094, 1001, 853, 741, 718, 689, 637, 596, 557, 436. ^{1}H NMR (500 MHz, $CDCl_3$, δ/ppm): 8.31 (d, *J* = 8.6 Hz, 2H), 8.18 (d, *J* = 7.9 Hz, 2H), 7.53 (s, 1H), 7.30 (s, 2H), 7.22 (s, 2H), 6.84 (s,

4H), 3.95 (s, $^{2}J_{Sn-H}$ = 153.3 Hz, 2H), 3.49 (s, 3H), 2.03 (s, 3H). ^{13}C NMR (126 MHz, d_6-DMSO, δ/ppm): 170.64, 161.06, 149.85, 146.58, 137.56, 135.91, 135.00, 131.56, 131.45, 131.25, 129.94, 129.78, 129.39, 127.78, 125.84, 125.73, 123.87, 48.52, 34.50 ($^{1}J_{Sn-C}$ = 1038.5 Hz), 19.71. ^{119}Sn NMR (187 MHz, d_6-DMSO, δ/ppm): -452.74. HRMS (ESI) m/z calcd for $C_{23}H_{19}ClN_3O_5Sn^+$ $[M\text{-}CH_3OH+H]^+$ 572.0030, found 572.0038.

[*p*-NO_2-C_6H_4(O)C=N-N=C(Ph)COO](\(CH_3OH\))(*p*-Cl-$C_6H_4CH_2$)SnCl (C6): Light yellow crystals, Yield 45%. m.p.: 144-146°C (dec.). FT-IR (KBr, cm^{-1}): 3113, 3082, 3059, 2940, 2778, 1665, 1609, 1593, 1528, 1479, 1445, 1387, 1344, 1323, 1290, 1258, 1171, 1155, 1090, 1013, 993, 870, 853, 833, 718, 691, 637, 596, 556, 476, 420, 401. ^{1}H NMR (500 MHz, $CDCl_3$, δ/ppm): 8.62 (s, 2H), 8.32 (d, J = 8.5Hz, 2H), 7.79 (d, J = 8.5Hz, 3H), 7.44 (d, J = 8.4Hz, 4H), 6.86 (s, 2H), 3.73 (s, $^{2}J_{Sn-H}$ = 153.6 Hz, 2H), 3.49 (s, 3H). ^{13}C NMR (126 MHz, d_6-DMSO, δ/ppm): 170.45, 161.32, 149.61, 146.71, 144.52, 137.97, 135.98, 131.32, 130.60, 129.69, 129.29, 128.99, 127.92, 127.58, 123.77, 48.50 ($^{1}J_{Sn-C}$ = 1041.2 Hz). ^{119}Sn NMR (187 MHz, d_6-DMSO, δ/ppm): -454.17. HRMS (ESI) m/z calcd for $C_{22}H_{16}Cl_2N_3O_5Sn^+$ $(M\text{-}CH_3OH+H)^+$ 591.9483, found 591.9484.

{[*p*-NO_2-C_6H_4(O)C=N-N=C(Ph)COO](*o*-Cl-$C_6H_4CH_2$)$_2$Sn(\(CH_3OH\)}$_2$ (C7): Red crystals, Yield 73%. m.p.: 102-104°C (dec.). FT-IR (KBr, cm^{-1}): 3451, 3057, 3019, 2936, 2826, 1636, 1607, 1591, 1528, 1501, 1474, 1439, 1387, 1344, 1288, 1256, 1169, 1157, 1086, 1015, 868, 851, 812, 750, 733, 719, 687, 633, 592, 573, 544, 440. ^{1}H NMR (500 MHz, $CDCl_3$, δ/ppm): 8.16 (d, J = 8.8Hz, 2H), 8.05 (s, 1H), 7.85-7.87 (m, 3H), 7.47-7.53 (m, 3H), 7.27-7.29 (m, 1H), 7.13-7.16 (m, 3H), 6.90-6.96 (m, 4H), 3.48 (s, 3H), 3.44 (d, J = 12.0 Hz, $^{2}J_{Sn-H}$ = 226.6 Hz, 2H), 3.33 (d, J = 12.0 Hz, $^{2}J_{Sn-H}$ = 226.6 Hz, 2H). ^{13}C NMR (126 MHz, $CDCl_3$, δ/ppm): 172.96, 163.54, 151.38, 149.87, 138.12, 124.40, 132.88, 131.73, 129.73, 130.62, 129.73, 129.04, 127.74, 127.35, 126.97, 126.83, 123.19, 50.88, 30.14 ($^{1}J_{Sn-C}$ = 573.6 Hz). ^{119}Sn NMR (187 MHz, $CDCl_3$, δ/ppm): -644.87. HRMS (ESI) m/z calcd for $C_{29}H_{22}Cl_2N_3O_5Sn^+$ $[M\text{-}CH_3OH+H]^+$ 681.9953, found 681.9953.

{[*p*-NO_2-C_6H_4(O)C=N-N=C(Ph)COO](2,4-Cl_2-$C_6H_3CH_2$)$_2$Sn(\(CH_3OH\)}$_n$ (C8): Yellow crystals, Yield 77%. m.p.: 122-124°C (dec.). FT-IR (KBr, cm^{-1}): 3618, 3231, 3055, 2945, 1622, 1578, 1526, 1499, 1472, 1385, 1342, 1292, 1256, 1173, 1155, 1109, 1088, 1045, 1013, 870, 853, 820, 762, 719, 691, 656, 592, 540, 442. ^{1}H NMR (500 MHz, $CDCl_3$,

δ/ppm): 8.19-8.22 (m, 2H), 7.85-7.88 (m, 4H), 7.55-7.80 (m, 3H), 7.19 (d, J = 2.1Hz, 2H), 7.10 (d, J = 8.4Hz, 2H), 6.93-6.95 (m, 2H), 3.50 (s, 3H), 3.43 (d, J = 12.0 Hz, $^{2}J_{Sn-H}$ = 114.4 Hz, 2H), 3.33 (d, J = 12.0 Hz, $^{2}J_{Sn-H}$ = 114.4 Hz, 2H). ^{13}C NMR (126 MHz, $CDCl_3$, δ/ppm):173.09, 163.42, 151.63, 150.02, 137.82, 133.40, 133.11, 132.39, 132.11, 131.72, 131.27, 129.35, 128.85, 128.16, 127.91, 127.33, 123.37, 50.90, 30.11 ($^{1}J_{Sn-C}$ = 607.2 Hz). ^{119}Sn NMR (187 MHz, $CDCl_3$, δ/ppm): -279.95. HRMS (ESI) m/z calcd for $C_{29}H_{20}Cl_4N_3O_5Sn^+$ $[M-CH_3OH+H]^+$ 749.9174, found 749.9151.

2.3 Single Crystal Structure Determination

X-ray diffraction data for crystals were performed with graphite monochromated Mo-Kα radiation (λ= 0.71073 Å) on a Bruker Smart Apex II CCD diffractometer, and collected by the φ-ω scan technique at ambient temperature. Multi-scan absorption correction was applied to the data. The crystal structures were solved by direct methods and refined by full-matrix least-squares on F^2. All the non-hydrogen atoms were located in successive difference Fourier syntheses and then refined anisotropically. Hydrogen atoms were placed in calculated positions or located from the Fourier maps, and refined isotropically with the isotropic vibration parameters related to the non-hydrogen atom to which they are bonded. All calculations were performed with SHELXL [35] programs within WINGX [36]. A summary of the crystallographic data and selected experimental information are given in Table S1. Crystallographic data for the structures of compounds reported in this paper have been deposited with the Cambridge Crystallographic Data Center as supplementary publication Nos. CCDC 1479715 (**C1**); 1479712 (**C2**); 1479716 (**C3**); 1479713 (**C4**); 1897744 (**C5**); 1897745 (**C6**); 1897746 (**C7**) and 1479714 (**C8**).

2.4 *In vitro* cytotoxic activity

NCI-H460(ATCC No: HTB-177), HepG2(ATCC No: HB-8065) and MCF-7(ATCC No: HTB-22) cells were obtained from American Tissue Culture Collection (ATCC). Normal human liver cell line (HL-7702) were obtained from the Shanghai Institute of Cell Biology, Chinese Academy of Sciences (Shanghai, China). The cells were maintained at 37°C in a 5% CO_2 incubator in RPMI 1640 (GIBICO, Invitrogen) containing 10% fetal bovine serum (GIBICO, Invitrogen). 5mM stock solutions of complexes were prepared in DMSO and diluted in fresh medium for use. The final concentration of DMSO never

exceeded 0.1% (v/v). Cell proliferation was assessed by MTT assay. 100 μL of cells (5×10^7 cells·L^{-1}) were seeded into 96 well plates. The cells incubated for 24 h at 37 °C, 5% CO_2. Then the medium was replaced with the respective medium containing complexes at different concentrations and incubated for 48 h. 10 μL of MTT was added and the medium was removed after 4 h of incubation. Finally, crystal violet was solubilized in 100 μL DMSO and the absorbance was measured at 570 nm. Six concentrations (10 nM-10 μM) were set for the compounds and at least 3 parallels of every concentration were used. All experiments were repeated at least three times. The data was calculated using Graph Pad Prism version 7.0. The IC_{50} were fitted using a non-linear regression model with a sigmoidal dose response [13].

2.5 Cell apoptosis assay

HepG2 and MCF-7 cells were seeded in sterile six-well plates at density of 1×10^8 cell·L^{-1} and 1×10^9 cell·L^{-1} (1mL per well), respectively. After the cells were attached for 24 h, the supernatant was discard. Then cells were exposed to **C2** solution at concentrations of 0.1, 0.3 and 0.5 uM. After 48 h incubation, the drugs were washed two times by cold PBS. Re-suspended cells in 100 ml binding buffer, Annexin V-PE (5 ml) and 7AAD (5 ml) were added to cells. And then cells were incubated for 15 min at room temperature in the dark and then analyzed by flow cytometry. Each group of experiments was measured in parallel 3 times [31].

2.6 Cell cycle analysis

HepG2 and MCF-7 cells were seeded in sterile six-well plates at density of 1×10^8 cell·L^{-1} and 1×10^9 cell·L^{-1} (1mL per well), respectively. After the cells were attached for 24 h, the supernatant was discard. Then cells were exposed to **C2** solution at concentrations of 0.1, 0.2 and 0.4 μM. After 48 h incubation, the drugs were washed two times by cold PBS. 70% ethanol was added. After the cells were fixed at 20°C overnight, RNaseA (10 μL) and PI (10 μL) were added to cells. And then cells were incubated for 15 min at room temperature in the dark and then detected by flow cytometry. Each group of experiments was measured in parallel 3 times [32].

2.7 DNA-binding studies

2.7.1 UV-visible absorption spectrometry

The investigation of the possible binding modes of complex to DNA and the calculation of the corresponding DNA-binding constants (K_b) were carried out by UV-vis

spectroscopy. UV-visible absorption spectrometry experiments were carried out with a constant concentration of **C2** (50 μM), and varying the concentration of CT-DNA (0-50 μM) in tris-HCl (0.01mol·L^{-1}) buffer solution. The intrinsic binding constants (K_b) was calculated according the following the Wolfe-Shimmer equation [37]:

$$c_{DNA} / (\varepsilon_A - \varepsilon_F) = c_{DNA} / (\varepsilon_B - \varepsilon_F) + 1 / K_b (\varepsilon_B - \varepsilon_F)$$

where c_{DNA} is the concentration of CT-DNA, ε_A is the observed extinction coefficient at arbitrary DNA concentration, ε_F is the extinction coefficient of the free complex, ε_B is the extinction coefficient of the complex when fully combinate to CT-DNA. The DNA-binding constants K_b were determined by the Wolfe-Shimmer equation and the plots $c_{DNA} / (\varepsilon_A - \varepsilon_F)$ versus c_{DNA}, K_b is given by the ratio of the slope to the intercept.

2.7.2 Fluorescence competitive study

In this fluorescence study, a mixture of the CT-DNA (30 μM), EB (30 μM) and different concentration complex **C2** solution (0-80 μM) was placed in a 5 mL volumetric flask in tris-HCl (0.01mol·L^{-1}) buffer solution. After 3 h, the fluorescence spectra were acquired at 25 °C. The excitation wavelength was 258 nm, and the emission wavelength is shown in spectrum. The slit scanning width of emission and excitation is 5.0 nm. Finally quenching constant (*K*sv) values of **C2** were determined by using Stern-Volmer equation [13].

2.7.3 Viscosity measurements

The viscosity measurements were carried out in the Ubbelohde viscometer, and it was keep in the water bath with 25.00 ± 0.02 °C. Viscosity experiments were performed by fixed DNA concentration (50 μM) and increasing the concentration of **C2** (0-50 μM) in tris-HCl (0.01mol·L^{-1}) buffer solution. The flow time of sample was measured with a digital stopwatch. The values of viscosity were calculated from the flow times of DNA containing solutions corrected for the flow time of buffer alone (t_0), $\eta = (t - t_0)$ [38]. Data was presented as $(\eta/\eta_0)^{1/3}$ versus $(c_{complex}/c_{DNA})$, where η is the viscosity of DNA in the presence of the complex, η_0 is the viscosity of DNA alone, $c_{complex}$ is the concentration of the complex and c_{DNA} is the concentration of DNA.

2.7.3 Gel electrophoresis studies

For the gel electrophoresis experiments, the gel electrophoresis experiments were performed by fixed pBR322 plasmid DNA concentration and increasing the concentration of **C2** (0, 20, 40, 60, 80, 100 μM), and the contents were incubated for 1 h at 25 °C. and they were electrophoresed for 1 h at 150 V on 1.0% agarose gel in TAE buffer (pH=8.0). Goldview was used for staining, the image was photographed by using gel imaging documentation system under UV light mode.

2.7.4 Molecular Docking.

Molecular docking was performed using MOE (Molecular Operating Environment) software. The crystal structure of DNA molecule was downloaded from Protein Data Bank (code: 453D)[39], and the embedded small molecule and water was removed by MOE software, hydrogenation was added to the DNA as it is required for the electrostatics, and point charge was calculated and the energy was minimized[40, 41]. The CIF file of complex is converted into a PDB file by Mercury 3.8 and imported into the MOE software, then removed the symmetrical unit and the coordinating solvent molecule, the energy minimized to obtain the complex for docking. Molecules docking results were obtained by Discovery Studio 3.5.

3 Results and discussion

3.1 Synthesis

The syntheses procedures are shown in Scheme 1. The organotin complexes (**C1-C8**) were synthesized by equimolar amounts of *p*-nitrobenzoylhydrazide, benzoylformic acid and the corresponding diorganotin halides or oxides under the microwave radiation, all reactant and solvent are added to the microware reaction kettle at one time, and after the reaction is finished, it is cooled to room temperature and then purified. The reaction time is 30 min. Obviously, the reaction operation is simple and efficient.

Through comparative experiments, we found that the yield of the complexes synthesized by traditional heating reflux method is not as good as that of microwave-assisted synthesis, and the yield of the stepwise synthesis is also not as high as that of the “one-pot”. So microware reaction has the characteristics of short reaction time, simple reaction step and good reproducibility.

In addition, it is easy to see that **C1-C4**, **C7** and **C8** are diorganotin complex in these complexes, **C5** and **C6** are monoorganotin compounds. The structures of the **C5** and **C6** are

different from the initial experimental design. It is speculated that the dehydrocarbyl reaction occurs during the reaction [42]. Initially, we suspected that it was related to microwave radiation, but the guess is not true after the comparison experiment, it found that **C5** and **C6** still obtained the dehydroalkylation product by the traditional heating reflux method. Therefore, it is suspected that the following factors may lead to dehydroalkylation: stronger nucleophiles than hydrocarbons attack the tin atoms, steric hindrance, charge density, etc. In summary, a more stable dehydrocarbyl compound is formed after removal of a alkyl group.

3.2 Spectroscopic Data Discussion

The wavenumbers (cm^{-1}) of different vibrational modes of of ligand (**H_2L**) and **C1-C8** was shown in the table 1. In the IR spectra of the complexes, a broad band in the range 3419-3618 cm^{-1} appearing in the **C2-C8**, as ν(OH) vibrations, indicating that methanol was involved in coordination. The gap between $\nu_{asym}(COO^-)$ and $\nu_{sym}(COO^-)$ is important to find out the binding mode of COO^- moiety with Sn atom. The literature [43] reveals the $\Delta[\nu_{asym}(COO^-)-\nu_{sym}(COO^-)]$ value in the range of 150-200 cm^{-1} indicates a bridging behaviour while a value >200 cm^{-1} exhibits monodentate coordination, other is considered to be practically bidentate. It was found that the $\Delta[\nu_{asym}(COO^-)-\nu_{sym}(COO^-)]$ value of **C2-C7** was 204-216 cm^{-1} by calculation. **C1** and **C8** are less than 200 cm^{-1}. Therefore, the coordination mode of COO^- and Sn atom in complexes **C2-C7** are monodentate coordination, the **C1** and **C8** are bridging coordination. The results of FT-IR study are consistent with the X-ray structure. Besides, the typical absorptions for Sn-C, Sn-N, Sn-O, Sn-O-Sn vibrations in the complexes are located in the normal range of similar organotin complexes [44, 45].

Table 1 The wavenumbers (cm^{-1}) of different vibrational modes of of ligand (**H_2L**) and **C1-C8**

Comp.	ν(OH)	$\nu_{asym}(COO^-)$	$\nu_{sym}(COO^-)$	ν(Sn-O-Sn)	ν(Sn-C)	ν(Sn-N)	ν(Sn-O)
H_2L	3271	~	~	~	~	~	~
C1	3421	1568	1384	690	592	547	449
C2	3419	1598	1382	690	594	542	429
C3	3568	1597	1383	696	594	552	459

C4	3482	1591	1383	691	592	546	461
C5	3107	1593	1385	689	596	557	436
C6	3113	1593	1387	691	596	556	476
C7	3451	1591	1387	687	592	554	440
C8	3618	1578	1385	691	592	540	442

The ^{1}H NMR spectrum show the ratio of the integral area of each group is consistent with the expected number of protons in each group [46]. It is observed that the substituted benzylic methylene protons in **C5** and **C6** were a normal single peak and a pair of small satellite peaks, this is the results of Sn-H coupling [47]. However, the substituted benzylic methylene protons in **C3**, **C4**, **C7** and **C8** were presenting two double peaks. From the analysis of single-crystal X-ray diffraction results, it is known the complexes **C5** and **C6** are a monobenzyltin compound and the complexes **C3**, **C4**, **C7** and **C8** are dibenzyltin, so it is speculated that the reason is that **C3**, **C4**, **C7** and **C8** cannot be freely rotated due to its large steric hindrance, resulting in the geminal coupling. Other hydrogen protons have similar chemical shifts in those complexes. The important ^{1}H NMR peak and their assignment of ligand (**H_2L**) and **C1**-**C8** was shown in the table 2.

Table 2 The important ^{1}H NMR peak and their assignment of ligand (**H_2L**) and **C1**-**C8**

Comp.	R	The important ^{1}H NMR peak (δ/ppm)
H_2L	-	12.92 (s, 1H, -COO**H**)
C1	Ph-	-
C2	*n*-Bu-	1.72-1.81 (m, 4H, -C**H**$_2$CH$_2$CH$_2$CH$_3$), 1.50-1.66 (m, 4H, -CH$_2$CH$_2$C**H**$_2$CH$_3$), 1.33-1.40 (m, 4H, -CH$_2$C**H**$_2$CH$_2$CH$_3$), 0.88 (t, *J* = 7.2 Hz, 6H, -CH$_2$CH$_2$CH$_2$C**H**$_3$)
C3	PhCH$_2$-	3.53 (d, *J* = 11.6 Hz, 2H, -C**H**$_2$Ph), 3.45 (d, *J* = 11.6 Hz, 2H, -C**H**$_2$Ph).
C4	*p*-Me-Ph-CH$_2$-	3.45 (d, *J* = 11.6 Hz, 2H, -C**H**$_2$Ph), 3.39 (d, *J* = 11.6 Hz, 2H, -C**H**$_2$Ph), 2.12 (s, 6H, -CH$_2$Ph-C**H**$_3$)
C5	*o*-Me-Ph-CH$_2$-	3.95 (s, 2H, -C**H**$_2$Ph), 2.03 (s, 3H, -CH$_2$Ph-C**H**$_3$).
C6	*p*-Cl-Ph-CH$_2$-	3.73 (s, 2H, -C**H**$_2$Ph).

C7	*o*-Cl-Ph-CH_2-	3.44 (d, *J* = 12.0 Hz, 2H, -C**H**$_2$Ph), 3.33 (d, *J* = 12.0 Hz, 2H, -C**H**$_2$Ph).
C8	2,4-Cl_2-Ph-CH_2-	3.43 (d, *J* = 12.0 Hz, 2H, -C**H**$_2$Ph), 3.33 (d, *J* = 12.0 Hz, 2H, -C**H**$_2$Ph)

In the ^{13}C NMR spectrum, the peaks of each group are consistent with the theoretical prediction of the number of carbon atoms in the structure [46]. The carboxyl carbon, hydrazide carbon and imino carbon of complexes can be clearly identified, they were located at the low field position. The peak positions of the all carbon atoms in the similar complexes are basically consistent.

In the ^{119}Sn spectrum, ^{119}Sn chemical shifts of the all complexes are observed. It presents only a sharp singlet, this indicates that the new complex has been generated and the R_2SnCl_2 or R_2SnO as a reactant is disappear.

3.3 Thermal stability

The thermal stabilities of both complexes were carried out from 40 to 800 °C at a rate of 20 °C min^{-1}, under an air atmosphere with a flowing rate of 20.0 mL·min^{-1}. As shown in Fig. S33~S40, the weight loss curves of **C2**~**C8** are relatively similar, three stages of weight loss can be observed, the mass loss in the first stage corresponds to the loss of the methanol molecules. However, only two weight loss stages were observed in **C1**, indicating that methanol was not involved in coordination, the results are consistent with the X-ray structure. The remaining weight indicates the final products are SnO_2 by calculation. In addition, as can be seen from the figure, all complex are stable up to about 100°C.

3.4 Crystal structure

The molecular structures of **C1**-**C8** are shown in Fig. 1. The geometric parameters of hydrogen bond in **C2**, **C3**, **C5**, **C6** and **C7** are in the Table 3. Selected bond lengths and bond angles of complexes are listed in Tables S2 (Supporting Information).

C1 shows a 16-membered macrocycle where four adjacent diphenyl tin centers are bridged to each other by the bridging 2-oxo-2-phenylacetic acid *p*-nitrobenzoyl hydrazide ligands to afford a tetranuclear. As can be seen from Fig. 1, all the tin atoms are distorted octahedral configuration, it is surrounded by two equatorial C atoms from phenyl groups and four axial O, N atoms from hydrazide ligands. The distances between the

symmetrically opposite tin centers in the macrocycle are 7.515 Å, it is worth mentioning that although the size of the cavity in the composite is large enough to capture some guest molecules, there are no small molecules in the cavity, and it is speculated that the cavity is almost completely occupied by the phenyl group on the tin atom.

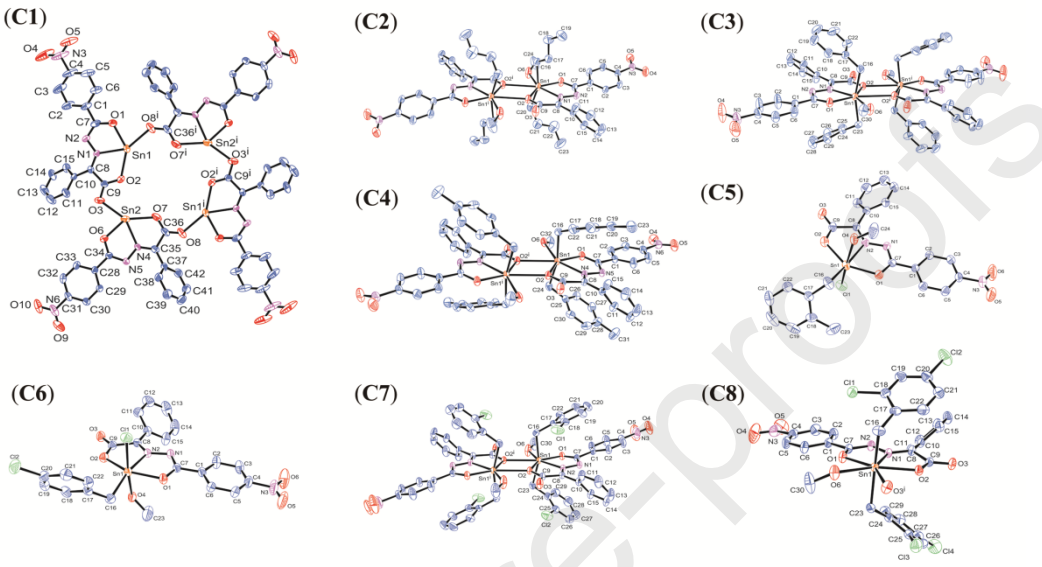

Fig.1 Molecular structure of **C1~ C8** (The phenyl group on the tin atom is omitted for clarity in **C1**.)

C2, **C3**, **C4** and **C7** are centrosymmetric dimer distannoxane, there is a Sn_2O_2 four-membered ring in the middle of the molecule, respectively. The center of the ring is the symmetry center of the molecule. In the four-membered Sn_2O_2 ring, the sum of the interior angles is 360°, indicating the four-membered Sn_2O_2 ring is planar. Each carboxyl oxygen atom bridges the two tin atoms in an antisymmetric unit, the Sn1-O2 bond belongs to the normal Sn-O covalent bond, The Sn1-O2^{i} bond distances (2.8395(22) Å **C2**; 2.8593(15) Å **C3**; 2.7595(12) Å **C4**; 2.6414(24) Å **C7**) are greater than covalent radii of Sn and O 2.13 Å, while are much less than the sum of the van der Waals radii 3.69 Å. Besides, **C2**, **C3** and **C7** form two-dimensional network structure and a one-dimensional band structure by weak action of C-H…O, respectively (Fig.2 (a), (b), (c)).

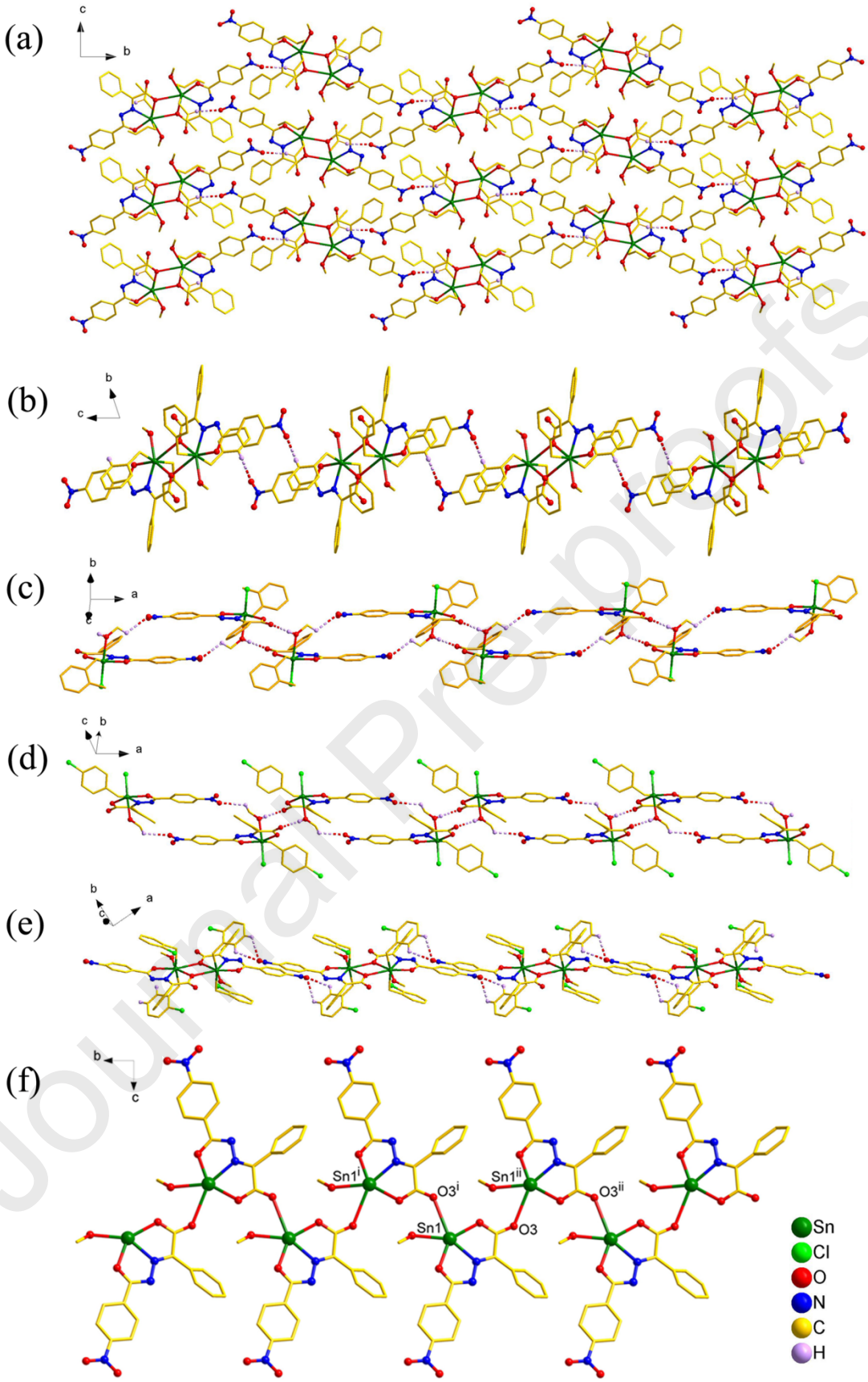

Fig.2 1D or 2D structures form by hydrogen bonds or Sn-O interaction in complexes (the 2,4-dichlorobenzyl group on the tin atom is omitted for clarity in (f))

C5 and **C6** are monomer structure and dehydroxylation products. The molecule structures of the **C5** and **C6** are almost the same, with only small differences in bond lengths and bond angles. **C5** and **C6** are monobenzyl tin compounds, and their central tin atoms are all six-coordinate in a distorted octahedral configuration and they form t a one-dimensional band structure by weak action of C-H…O and O-H…O, respectively (Fig.2 (d), (e)). The bond lengths of C-H…O and O-H…O are not much different from the literature report [48-50].

In the complex **C8**, the central tin atoms are all seven coordination of the distorted pentagonal bipyramidal configuration. It is worth noting that the bond length of Sn1-O3^{i} is 2.9415(21) Å, which is much less than the sum of the Van der Waals radii for Sn and O, it proves that there is a strong interaction between Sn1 and O3^{i}. So the one-dimensional infinite chain structure is formed by Sn1-O3^{i} (Fig.2 (f)). In the one-dimensional infinite chain of **C8**, each asymmetric unit contains two *p*-NO_2-C_6H_4-(O)C=N-N=C(Ph)COO](CH$_3$OH)(2,4-Cl_2-$C_6H_3CH_2)_2$Sn with a pitch of 10.2876(7) Å. The distance between two adjacent Sn atoms is 6.4394(4) Å and the Sn atoms are arrange in a relationship with the Sn…Sn…Sn angle of 106.032(4)°.

Table 3 Geometric parameters of hydrogen bond in **C2**, **C3**, **C5**, **C6** and **C7**

Comp.	D-H…A	Distance, Å			Angle DHA, °
		D-H	H…A	D…A	
C2	C17-H17B…O4^{i}	0.970	2.579	3.482	155.08
C3	C29-H29…O5^{i}	0.930	2.526	3.239	166.91
C5	O4-H4A…O3^{i}	0.738	1.863	2.589	168.26
	C24-H24A…O6^{i}	0.960	2.656	3.150	112.48
C6	O4-H4A…O3^{i}	0.673	1.963	2.635	177.30
	C23-H23B…O6^{i}	0.969	2.639	3.240	121.10
C7	C28-H28…O5^{i}	0.931	2.705	3.310	123.46
	C29-H29…O5^{i}	0.931	2.715	3.319	123.34

3.5 Cell-cytotoxicity assays

Complexes **C1-C8** and carboplatin were evaluated for cytotoxicity *in vitro* by MTT assay against human non-small cell lung cancer (NCI-H460), human breast

adenocarcinoma (MCF-7) and human liver hepatocellular carcinoma (HepG2) cell lines. Table 4 lists the cytotoxicity screening results for all organotin complexes. The complexes **C1** and **C2** exerted strong cytotoxic effects against tested cancer cell lines with a lower IC_{50} value (<2.0 μM), and better than the positive control drug Carboplatin. The complexes **C3**, **C4**, **C7** and **C8** showed moderate cytotoxicity. The complexes **C5** and **C6** did not show 50% inhibition at a concentration of 10 μM. Among these cell lines, the HepG2 cell line was the most sensitive towards **C2** with IC_{50} values of 0.28 ± 0.06 μM, and the MCF-7 cell is second (IC_{50}=0.67 ± 0.07). They have a lower IC_{50} value than the anticancer activity of other organotin compounds [51-54].

Table 4 The cytotoxicity of complexes(**C1-C8**) *in vitro*.

Comp.	IC_{50} / μM			
	NCI-H460	MCF-7	HepG2	HL-7702
C1	1.91 ± 0.12	1.51 ± 0.09	1.14 ± 0.08	
C2	1.18 ± 0.03	0.67 ± 0.07	0.28 ± 0.06	4.25 ± 0.06 (15.17) [b]
C3	5.74 ± 0.14	3.92 ± 0.23	3.65 ± 0.11	
C4	4.50 ± 0.09	3.06 ± 0.04	2.74 ± 0.17	
C5	>10[a]	>10	>10	
C6	>10	>10	>10	
C7	7.26 ± 0.15	3.24 ± 0.09	4.36 ± 0.09	
C8	8.73 ± 0.21	4.90 ± 0.17	4.52 ± 0.07	
Carboplatin	7.26 ± 0.32	8.22 ± 0.41	7.70 ± 0.25	

[a] Because of the limited solubility of complexes, the maximum concentration of complexes can only reach 10 μM.

[b] The selectivity index factor, defined as IC_{50} (normal HL-7702 cells)/IC_{50} (HepG2 cancer cells), is given in parentheses.

Based on this observation, possible structure-activity relationship can be recognized as follows: dibutyltin complex > diphenyltin complex > dibenzyltin complex > monobenzyltin complex. It can be presumed that the number of alkyl substituted on tin played a key role in the killing of cancer cells. **C5** and **C6** are monobenzyltin complex,

their tumor cytotoxicity are inferior to other diorganotin complexes. However, in diorganotin complexes, the difference in cytotoxicity might be attributed to the small steric hindrance or small molecular weight. This trend is in accordance with the results reported in the literature [55, 56].

To gain more insights into the possible *in vitro* cytoselectivity of **C2** with the high cytotoxicity for HepG2 and MCF-7 cell line, MTT assays were also performed in normal human liver cells (HL-7702) (Table 1). **C2** shows the lower cytotoxic activity in the normal human liver cells line (IC_{50} = 4.25 ± 0.06 μM) than in HepG2 cell line (IC_{50} = 0.28 ± 0.06 μM), which demonstrates the obvious specificity for this type of tumor cell and high selectivity index factors of more than 3.0 [57-59]. So the complex **C2** may be used as a candidate compound for the anticancer drug after further chemical optimization.

3.6 Cell apoptosis analysis by flow cytometry

Table 5 The percentages of apoptosis of **C2** in different concentrations.

Cell	Comp.	Concentration (μM)	Q2 (late apoptosis and necrotic cell)	Q4 (early apoptosis)	Total percentage
HepG2	Control		0.64	0.31	0.95
	C2	0.1	2.40	0.82	3.22
		0.3	21.75	5.76	27.51
		0.5	40.94	11.00	51.94
MCF-7	Control		4.11	0.82	4.93
	C2	0.1	5.53	0.43	5.96
		0.3	19.82	1.77	21.59
		0.5	36.97	1.89	37.86

On the basis of the cytotoxicity effect study, **C2** with good activity was selected for further experiments. Since **C2** has a better inhibitory activity against HepG2 and MCF-7 cells, we performed a flow cytometry assay to determine the level of apoptosis of HepG2 and MCF-7 cells exposed to **C2**. Early stages of apoptosis are characterized by perturbations in the cellular membrane. It leads to a redistribution of phosphatidylserine (PS) to the external side of the cell membrane, which causes a Ca flux. Annexin V is a Ca-dependent phospholipidbinding protein with high affinity for PS. Therefore,

fluorescently labeled annexin V can be used to identify early apoptosis cells[32]. The percentage of apoptosis was presented in Table 5 and Fig. 3 by the region Q4 (early apoptosis) and Q2 (late apoptosis and necrotic cell) and total percentages of apoptosis. We can see that **C2** did not significantly induce apoptosis of HepG2 and MCF-7 cells at low concentrations (0.1 μM). With the increase of the concentration of **C2**, the apoptosis induction obviously increased. The total apoptosis percentages are 27.51%, 51.94% (HepG2) and 21.59%, 38.86% (MCF-7) at the concentration of 0.3 and 0.5 μM, respectively, which are also higher than the control. These data show **C2** is able to induce HepG2 or MCF-7 cancer cell apoptosis at some extent, which might partially related to the strong antitumor activity of **C2**.

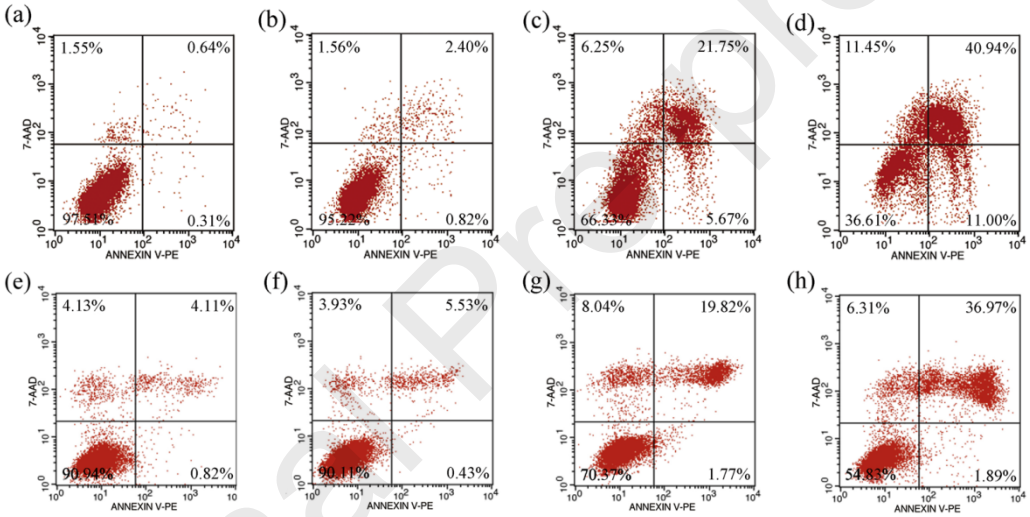

Fig. 3 Effect of **C2** on apoptosis of HepG2 (a~d) and MCF-7 cells (e~h). Apoptosis detection in HepG2 and MCF-7 cells using the Annexin V assay after 24 h. The total percentage of apoptotic cells was considered as Q2 + Q4. Plot presents the fluorescence data of 7-aminoactinomycin D (7-AAD) and Annexin V fluorescein corresponding to (a) 0.95% (control) apoptotic cells, (b) 3.22% (0.1 μM), (c) 27.51% (0.3 μM), (d) 51.94% (0.5 μM), (e) 4.93% (control) apoptotic cells, (f) 5.96% (0.1 μM), (g) 21.59% (0.3 μM), (h) 38.86% (0.5 μM).

3.7 Cell cycle distribution analysis by flow cytometry

Table 6 Cell populations of HepG2 and MCF-7 cells after treating by **C2**

Cell	Comp.	Concentration (μM)	G_0/G_1 (%)	G_2/M (%)	S (%)
HepG2	Control		67.69	10.43	21.88

	C2	0.1	64.58	10.98	24.44
		0.2	61.51	10.55	27.94
		0.4	55.42	8.55	36.03
	Control		65.80	12.62	21.57
MCF-7	**C2**	0.1	63.31	11.03	25.67
		0.2	57.72	14.01	28.27
		0.4	59.20	9.95	30.85

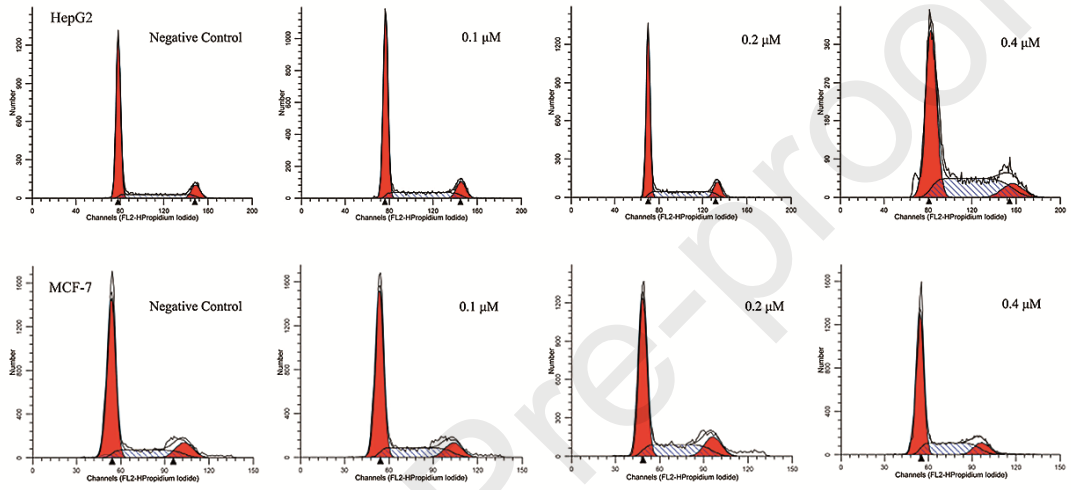

Fig. 4 Effects of **C2** on cycle of HepG2 and MCF-7. HepG2 and MCF-7 cells were exposed various concentrations (0.1-0.4 μM) of **C2** in 24 h, and the cells were harvested and flow cytometry analyzed for cell cycle distribution by propidium iodide (PI) staining.

Cell cycle analysis was performed to investigate the anti-proliferative effects of the **C2**. Difference between phases of the cell cycle is based on the content of genetic material. The cell population in the S phase (DNA replication phase) is synthesizing genetic material, and thus contains more DNA than quiescent cells. The subsequent G2/M phase (interphase/mitosis) is characterized by the presence of two copies of DNA [31]. Therefore, changes in these stages are used as a basis for the treatment of cancer. In order to study DNA cell content changes in cell cycle, cell cycle analysis was performed by PI single labeling (Fig. 4). This experiment found that the **C2** can change the cell cycle distribution of HepG2 and MCF-7 (Table 6). Compared with the control group, as the concentration increases, the proportion of cells in the G2/M phase is reduced, the proportion of cells in the S phase significantly increased. Apoptosis rate is also significantly improved. It is

suggested that the **C2** can arrest the cell cycle in the S phase, and block the progression of cancer cells from the S phase to the G2/M phase, so that block the mitosis of the cells. The **C2** induces apoptosis by inhibiting DNA replication and transcription, and achieves an anti-tumor effect. Significantly, the cell cycle arrest at S phase of **C2** is entirely different from reported dibutyltin complexes [24, 31] or platinum-based chemotherapy drug [60, 61].

3.8 DNA-binding studies

3.8.1 UV-visible absorption spectrometry

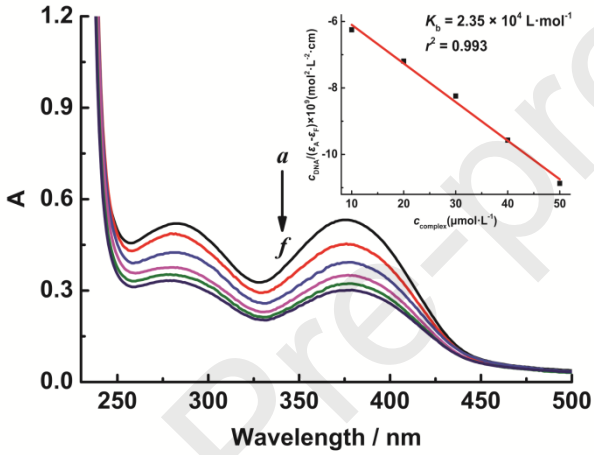

Fig. 5 Electronic spectra of **C2** in Tris-HCl buffer upon addition of CT-DNA, $c_{complex}$ = 50 μmol·L^{-1}; from *a* to *f*, c_{DNA} = 0, 10, 20, 30, 40, 50 μmol·L^{-1}, respectively. The arrow shows the absorbance changes upon increasing DNA concentrations. Inset: plot of $c_{DNA}/(\varepsilon_A - \varepsilon_F)$ *vs* $c_{complex}$.

The electronic absorption spectra of **C2** in the absence and presence of CT-DNA are shown in Fig.5. It can be seen from the Fig.5 that the decrease in absorbance occurs with the increase of DNA concentration. Hypochromism occurs own to the breakage of the secondary structure of DNA, whereas hypochromism is due to the stabilization of DNA duplex through a strong interaction such as intercalation.

From the absorption spectroscopy tests, K_b values of **C2** were calculated as 2.35×10^4 L·mol^{-1} (r^2 = 0.993), as can be seen that it is similar to the reported complexes in the literature [62, 63], and it explained the intercalation of complexes and DNA are relatively stronger. It preliminary indicated there are intercalation in the interaction of between the **C2** and the DNA.

3.8.2 Fluorescence competitive study

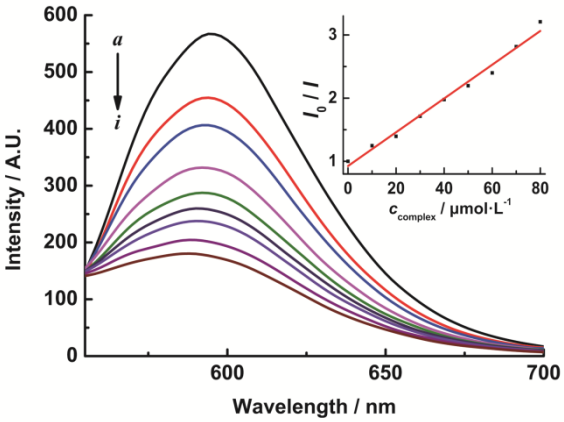

Fig. 6 Effects of complex **C2** on the fluorescent spectra of EB-DNA system, c_{DNA} = 30 μmol·L^{-1}; c_{EB} = 3 μmol·L^{-1}; from *a* to *i*, $c_{complex}$ = 0, 10, 20, 30, 40, 50, 60, 70, 80 μmol·L^{-1}, respectively. The arrow shows the emission intensity changes upon increasing DNA concentrations. Inset: plot of I_0/I *vs* $c_{complex}$, λ_{ex} = 258nm.

Fig.6 is fluorescence quenching curve of different concentration **C2** on the EB-DNA system. The fluorescence of EB-DNA system was obviously decreased after the addition of **C2**, it is showed that the presence of **C2** makes the fluorescence of EB-DNA system quenched. The fluorescence quenching is up to 68.8% of the initial EB-DNA fluorescence intensity indicating the competition of the complex with EB in the binding to DNA. The results show **C2** may displace EB from the DNA-EB, interacting with DNA by the intercalative mode. According to Stern-Volmer correction equation [64]: I_0/I=1+$K_{SV}c_{complex}$, the K_{SV} was calculated as 2.54×10^4 L·mol^{-1}, this value is larger than the reported in the literature [65, 66]. It indicated that the **C2** has a strong intercalation with DNA, and can be assumed that the tin atom of **C2** combined the base pairs of DNA, the terminal ligands inserted into the DNA base pairs to compete with EB, so that EB is squeeze out the DNA double helix by **C2**.

3.8.3 Viscosity measurements

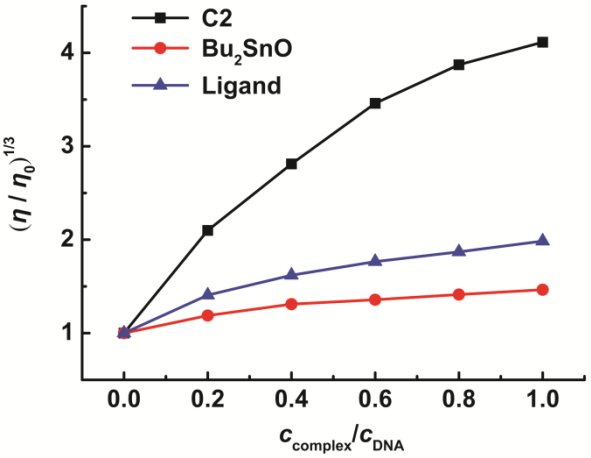

Fig. 7 Effect of increasing amounts of the complex **C2**, Bu_2SnO and Ligand on the relative viscosity at 25.00 ± 0.02 °C

Viscosity experimental results clearly showed that the relative viscosity of CT-DNA steadily increasing with concentration of **C2**, however, this trend is unconspicuous in Bu_2SnO and ligand. The literature [55, 67] reported that a significant increase in the viscosity of DNA on the addition of a complex indicates the classical intercalative mode of binding to DNA. In contrast, if the interaction of the complex with the DNA is caused by partial or non-classical insertion, the viscosity change of the DNA solution is not obvious or unchanged. As can be seen from the Fig.7, the order of increase in viscosity is **C2** > Ligand > Bu_2SnO. This observation can be explained by the fact that the **C2** and DNA adopt a classical intercalation model, which requires that the DNA helix must be extended, resulting in an increase in DNA viscosity. The result further suggests an intercalating binding mode of the complexes with DNA and also parallels the above spectroscopic results.

3.8.4 Gel electrophoresis studies

The effect of complex on DNA cleavage was studied by agarose gel electrophoresis. The activity depends mainly on the properties, concentration and reaction time of the complex itself. When the complex interacts with the supercoiled plasmid DNA, the closed-loop supercoiled structure (Form I) becomes an open-loop notch type (Form II) if it causes a gap in one strand of the closed-loop supercoil, and when two chains break at the same position, they become linear structures (Form III) [68]. The migration rate of the three kinds of plasmid DNA in agarose gel electrophoresis is different. The closed-loop

supercoiled (Form I) moves closer to the front through the gel due to its tight structure, followed by the linear structures (Form III). The open-loop notch type (Form II) is restrained due to its loose structure, and the movement to the positive electrode is suppressed. As can be seen from the Fig.8, upon increasing concentrations of **C2** from 0, 20, 40, 60, 80, 100μmol·L^{-1}, the effect on DNA mobility was negligible and even at highest concentration the complex was able to cleave the DNA, and it can convert pBR322 from Form I to Form II, and the DNA fracture degree increased with increasing complex concentration. It explain that **C2** have higher cleavage activity and is well inserted into DNA.

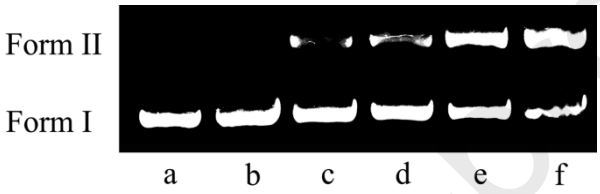

Fig. 8 Agarose gel electrophoresis of pBR322 treated with different concentrations **C2**, from *a* to *f*, $c_{complex}$ = 0, 20, 40, 60, 80, 100 μmol·L^{-1}, respectively.

3.8.5 Molecular Docking

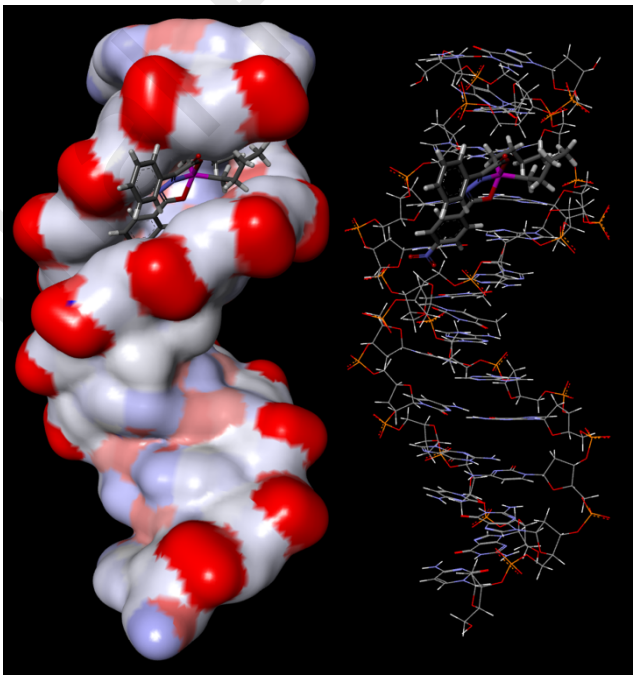

Fig.9 Molecular modeling of the interaction between **C2** and DNA

Molecular docking can obviously express the characteristic information of the interaction between complex and DNA, and guide us to understand the binding mode of

DNA and complex from the molecular level. From Fig. 9, the docking results showed that **C2** bind to DNA by intercalation. It can be seen that the whole **C2** molecule inserted into the double helix of DNA. It suggested that **C2** was capable of binding to DNA through intercalation binding. So docking studies revealed that **C2** interacted with DNA through intercalation binding which was also in accordance with spectroscopic investigations.

Based on the anti-cancer activity data, it is speculated from the docking results that the whole molecule structure of **C2** can be embedded in the base pair of DNA and reversibly bind to the double helix of DNA, resulting in DNA cleavage. And transcription and synthesis of DNA is affected, so the anti-tumor effect is finally achieved.

4. Conclusions

Diorganotin complexes (**C1, C2, C3, C4, C7, C8**) have better in vitro anticancer activity than monoorganotin complexes (**C5, C6**). Among these complexes, dibutyltin complex **C2** has an exceptionally high anticancer activity against HpeG2 and MCF-7 cells. In the past, dibutyltin complexes were considered to be a cell cycle nonspecific agent, as were platinum-based chemotherapy drugs. However, it was found that the dibutyltin complex of 2-oxo-2-phenylacetic acid *p*-nitrobenzoyl hydrazide (**C2**) is a cell cycle specific agents through flow cytometry in this paper. It can block HpeG2 and MCF-7 cells in S phase and eventually causes apoptosis. In further experiments, it was found that **C2** can be well embedded in the double helix of DNA and cleave DNA. This indicates that **C2** inhibits DNA synthesis of cancer cells by binding to DNA, so as to inhibit the growth of cancer cells. In summary, the **C2** may be a potential candidate for further chemical optimization and cancer therapy.

Acknowledgements

This work was supported by the Science and Technology Development Plan Project of Hengyang City (grant number: 2018KJ121); Hengyang Normal University Industrial Supported Project (grant number: HXKJ201908, HXKJ201911, HXKJ201946, HXKJ201947); and the Foundation of Key Laboratory of Functional Organometallic Materials, University of Hunan Province (grant number: GN19K07).

Appendix A. Supplementary material

Supplementary Material Crystallographic data for the structural analysis have been deposited with the Cambridge Crystallographic Data Centre, CCDC No. 1479715 (**C1**); 1479712 (**C2**); 1479716 (**C3**); 1479713 (**C4**); 1897744 (**C5**); 1897745 (**C6**); 1897746 (**C7**) and 1479714 (**C8**).

References

[1] B. Rosenberg, L. Vancamp, J.E. Trosko, V.H. Mansour, Platinum Compounds: a New Class of Potent Antitumour Agents, Nature 222 (1969) 385-386.

[2] S. Dasari, P. Bernard Tchounwou, Cisplatin in cancer therapy: Molecular mechanisms of action, Eur. J. Pharmacol. 740 (2014) 364-378.

[3] F. Shahid, Z. Farooqui, F. Khan, Cisplatin-induced gastrointestinal toxicity: An update on possible mechanisms and on available gastroprotective strategies, Eur. J. Pharmacol. 827 (2018) 49-57.

[4] A. Rajeswaran, A. Trojan, B. Burnand, M. Giannelli, Efficacy and side effects of cisplatin- and carboplatin-based doublet chemotherapeutic regimens versus non-platinum-based doublet chemotherapeutic regimens as first line treatment of metastatic non-small cell lung carcinoma: A systematic review of randomized controlled trials, Lung Cancer-j. Iaslc. 59 (2008) 1-11.

[5] J.H. van den Berg, J.H. Beijnen, A.J.M. Balm, J.H.M. Schellens, Future opportunities in preventing cisplatin induced ototoxicity, Cancer Treat. Rev. 32 (2006) 390-397.

[6] J.A. Levi, R.S. Aroney, D.N. Dalley, Haemolytic anaemia after cisplatin treatment, British medical journal (Clinical research ed.) 282 (1981) 2003-2004.

[7] T. Karasawa, P.S. Steyger, An integrated view of cisplatin-induced nephrotoxicity and ototoxicity, Toxicol. Lett. 237 (2015) 219-227.

[8] N. Milosavljevic, C. Duranton, N. Djerbi, P.H. Puech, P. Gounon, D. Lagadic-Gossmann, M.T. Dimanche-Boitrel, C. Rauch, M. Tauc, L. Counillon, M. Poët, Nongenomic Effects of Cisplatin: Acute Inhibition of Mechanosensitive Transporters and Channels without Actin Remodeling, Cancer Res. 70 (2010) 7514-7522.

[9] D.J. Stewart, Mechanisms of resistance to cisplatin and carboplatin, Critical Reviews in Oncology/Hematology 63 (2007) 12-31.

[10] B. Köberle, M.T. Tomicic, S. Usanova, B. Kaina, Cisplatin resistance: Preclinical findings and clinical implications, Biochimica et Biophysica Acta (BBA) - Reviews on Cancer 1806 (2010) 172-182.

[11] L. Amable, Cisplatin resistance and opportunities for precision medicine, Pharmacol. Res. 106 (2016) 27-36.

[12] M.Z. Bulatović, D. Maksimović-Ivanić, C. Bensing, S. Gómez-Ruiz, D. Steinborn, H. Schmidt, M. Mojić, A. Korać, I. Golić, D. Pérez-Quintanilla, M. Momčilović, S. Mijatović, G.N. Kaluđerović, Organotin(IV)-Loaded Mesoporous Silica as a Biocompatible Strategy in Cancer Treatment, Angew. Chem. Int. Ed. 53 (2014) 5982-5987.

[13] M. Hong, H. Geng, M. Niu, F. Wang, D. Li, J. Liu, H. Yin, Organotin(IV) complexes derived from Schiff base N′-[(1E)-(2-hydroxy-3-methoxyphenyl)methylidene]pyridine-4-carbohydrazone: Synthesis, in vitro cytotoxicities and DNA/BSA interaction, Eur. J. Med. Chem. 86 (2014) 550-561.

[14] M. Nath, P.K. Saini, Chemistry and applications of organotin(iv) complexes of Schiff bases, Dalton. Trans. 40 (2011) 7077-7121.

[15] H. Wang, L. Hu, W. Du, X. Tian, Q. Zhang, Z. Hu, L. Luo, H. Zhou, J. Wu, Y. Tian, Two-Photon Active Organotin(IV) Carboxylate Complexes for Visualization of Anticancer Action, ACS Biomaterials Science & Engineering 3 (2017) 836-842.

[16] R.G. Kenny, C.J. Marmion, Toward Multi-Targeted Platinum and Ruthenium Drugs—A New Paradigm in Cancer Drug Treatment Regimens?, Chem. Rev. 119 (2019) 1058-1137.

[17] Y.K. Yan, M. Melchart, A. Habtemariam, P.J. Sadler, Organometallic chemistry, biology and medicine: ruthenium arene anticancer complexes, Chem. Commun. 0 (2005) 4764-4776.

[18] W. Cao, J. Qi, K. Qian, L. Tian, Z. Cheng, Y. Wang, Structure−activity relationships of 2-quinolinecarboxaldehyde thiosemicarbazone gallium(III) complexes with potent and selective anticancer activity, J. Inorg. Biochem. 191 (2019) 174-182.

[19] A.R. Timerbaev, Advances in developing tris(8-quinolinolato)gallium(iii) as an anticancer drug: critical appraisal and prospects, Metallomics 1 (2009) 193-198.

[20] P.M. Abeysinghe, M.M. Harding, Antitumour bis(cyclopentadienyl) metal complexes: titanocene and molybdocene dichloride and derivatives, Dalton. Trans. (2007) 3474-3482.

[21] D. Díaz-García, D. Cenariu, Y. Pérez, P. Cruz, I. del Hierro, S. Prashar, E. Fischer-Fodor, S. Gómez-Ruiz, Modulation of the mechanism of apoptosis in cancer cell lines by treatment with silica-based nanostructured materials functionalized with different metallodrugs, Dalton. Trans. 47 (2018) 12284-12299.

[22] A.J. Salmon, M.L. Williams, Q.K. Wu, J. Morizzi, D. Gregg, S.A. Charman, D. Vullo, C.T. Supuran, S.-A. Poulsen, Metallocene-Based Inhibitors of Cancer-Associated Carbonic Anhydrase Enzymes IX and XII, J. Med. Chem. 55 (2012) 5506-5517.

[23] M. Zaki, S. Hairat, E.S. Aazam, Scope of organometallic compounds based on transition metal-arene systems as anticancer agents: starting from the classical paradigm to targeting multiple strategies, RSC Advances 9 (2019) 3239-3278.

[24] A. Attanzio, M. Ippolito, M.A. Girasolo, F. Saiano, A. Rotondo, S. Rubino, L. Mondello, M.L. Capobianco, P. Sabatino, L. Tesoriere, G. Casella, Anti-cancer activity of di- and tri-organotin(IV) compounds with D-(+)-Galacturonic acid on human tumor cells, J. Inorg. Biochem. 188 (2018) 102-112.

[25] T.S. Basu Baul, A. Paul, L. Pellerito, M. Scopelliti, P. Singh, P. Verma, A. Duthie, D. de Vos, E.R.T. Tiekink, Dibutyltin(IV) complexes containing arylazobenzoate ligands: chemistry, in vitro cytotoxic effects on human tumor cell lines and mode of interaction with some enzymes, Invest. New Drug 29 (2011) 285-299.

[26] X. Shang, X. Meng, E.C.B.A. Alegria, Q. Li, M.F.C. Guedes da Silva, M.L. Kuznetsov, A.J.L. Pombeiro, Syntheses, Molecular Structures, Electrochemical Behavior,

Theoretical Study, and Antitumor Activities of Organotin(IV) Complexes Containing 1-(4-Chlorophenyl)-1-cyclopentanecarboxylato Ligands, Inorg. Chem. 50 (2011) 8158-8167.

[27] A.J. Crowe, P.J. Smith, G. Atassi, Investigations into the antitumour activity of organotin compounds. I. Diorganotin dihalide and di-pseudohalide complexes, Chem-biol. Interact. 32 (1980) 171-178.

[28] H.-z. Xuan, J.-h. Zhang, Y.-h. Wang, C.-l. Fu, W. Zhang, Anti-tumor activity evaluation of novel chrysin–organotin compound in MCF-7 cells, Bioorg. Med. Chem. Lett 26 (2016) 570-574.

[29] T.S. Basu Baul, S. Basu, D. de Vos, A. Linden, Amino acetate functionalized Schiff base organotin(IV) complexes as anticancer drugs: synthesis, structural characterization, and in vitro cytotoxicity studies, Invest. New Drug 27 (2008) 419.

[30] F. Shaheen, M. Sirajuddin, S. Ali, R. Zia ur, P.J. Dyson, N.A. Shah, M.N. Tahir, Organotin(IV) 4-(benzo[d][1,3]dioxol-5-ylmethyl)piperazine-1-carbodithioates: Synthesis, characterization and biological activities, J. Organomet. Chem. 856 (2018) 13-22.

[31] X. Shang, N. Ding, G. Xiang, Novel di-n-butyltin(IV) derivatives: Synthesis, high levels of cytotoxicity in tumor cells and the induction of apoptosis in KB cancer cells, Eur. J. Med. Chem. 48 (2012) 305-312.

[32] B. Zhao, X. Shang, L. Xu, W. Zhang, G. Xiang, Novel mixed ligand di-n-butyltin(IV) complexes derived from acylpyrazolones and fluorinated benzoic acids: Synthesis, characterization, cytotoxicity and the induction of apoptosis in Hela cancer cells, Eur. J. Med. Chem. 76 (2014) 87-97.

[33] T.S. Basu Baul, D. Dutta, A. Duthie, N. Guchhait, B.G.M. Rocha, M.F.C. Guedes da Silva, R.B. Mokhamatam, N. Raviprakash, S.K. Manna, New dibutyltin(IV) ladders: Syntheses, structures and, optimization and evaluation of cytotoxic potential employing A375 (melanoma) and HCT116 (colon carcinoma) cell lines in vitro, J. Inorg. Biochem. 166 (2017) 34-48.

[34] Y.-l. Li, Z.-w. Wang, P. Guo, L. Tang, R. Ge, S.-r. Ban, Q.-y. Chai, L. Niu, Q.-s. Li, Diorganotin(IV) derivatives of substituted N-hydroxybenzamides with selective cytotoxicity in vitro and potent antitumor activity in vivo, J. Inorg. Biochem. 133 (2014) 1-7.

[35] G.M. Sheldrick, SHELXL-97, A Program for Crystal Structure Refinement., University of Geöttingen, Germany Geöttingen, 1997.

[36] L.J. Farrugia, WINGX: A Windows Program for Crystal Structure Analysis, University of Glasgow, Glasgow, 1988.

[37] A.M. Pyle, J.P. Rehmann, R. Meshoyrer, C.V. Kumar, N.J. Turro, J.K. Barton, Mixed-ligand complexes of ruthenium(II): factors governing binding to DNA, J. Am. Chem. Soc. 111 (1989) 3051-3058.

[38] C. Tan, J. Liu, L. Chen, S. Shi, L. Ji, Synthesis, structural characteristics, DNA binding properties and cytotoxicity studies of a series of Ru(III) complexes, J. Inorg. Biochem. 102 (2008) 1644-1653.

[39] S. Neidle, E. L. Rayner, I. J. Simpson, N. J. Smith, J. Mann, A. Baron, Y. Opoku-Boahen, K. R. Fox, J. A. Hartley, L. R. Kelland, Symmetric bis-benzimidazoles: new

sequence-selective DNA-binding molecules, Chem. Commun. (1999) 929-930.

[40] Z. Su, W. Tian, J. Li, C. Wang, Z. Pan, D. Li, H. Hou, Biological evaluation and molecular docking of Rhein as a multi-targeted radiotherapy sensitization agent of nasopharyngeal carcinoma, J. Mol. Struct. 1147 (2017) 462-468.

[41] Z. Su, Z. Li, C. Wang, W. Tian, F. Lan, D. Liang, J. Li, D. Li, H. Hou, A novel Rhein derivative: Activation of Rac1/NADPH pathway enhances sensitivity of nasopharyngeal carcinoma cells to radiotherapy, Cell Signal. 54 (2019) 35-45.

[42] V. Chandrasekhar, K. Gopal, P. Sasikumar, R. Thirumoorthi, Organooxotin assemblies from Sn-C bond cleavage reactions, Coordin. Chem. Rev. 249 (2005) 1745-1765.

[43] G.B. Deacon, R.J. Phillips, Relationships between the carbon-oxygen stretching frequencies of carboxylato complexes and the type of carboxylate coordination, Coordin. Chem. Rev. 33 (1980) 227-250.

[44] M.A. Salam, M.A. Hussein, I. Ramli, M.S. Islam, Synthesis, structural characterization, and evaluation of biological activity of organotin(IV) complexes with 2-hydroxy-5-methoxybenzaldehyde-N(4)-methylthiosemicarbazone, J. Organomet. Chem. 813 (2016) 71-77.

[45] M. Hong, H. Yin, X. Zhang, C. Li, C. Yue, S. Cheng, Di- and tri-organotin(IV) complexes with 2-hydroxy-1-naphthaldehyde 5-chloro-2-hydroxybenzoylhydrazone: Synthesis, characterization and in vitro antitumor activities, J. Organomet. Chem. 724 (2013) 23-31.

[46] E. Pretsch, P. Bühlmann, M. Badertscher, Structure Determination of Organic Compounds, Fourth ed., Springer-Verlag Berlin Heidelberg, 2009.

[47] A.G. Davies, Organotin Chemistry, second ed., Wiley-VCH Verlag GmbH & Co. KGaA, Weinheim, 2004.

[48] S.E.-d.H. Etaiw, M.M. El-bendary, Crystal structure, characterization and catalytic activities of Cu(II) coordination complexes with 8-hydroxyquinoline and pyrazine-2-carboxylic acid, Appl. Organomet. Chem. 32(4) (2018) e4213.

[49] S.E.-d.H. Etaiw, M.M. El-bendary, Hydrogen bonded 3D-network of silver and 2,6-pyridinedicarboxylic acid complex: Structure and applications, J. Mol. Struct. 1173 (2018) 7-16.

[50] M.M. El-bendary, T. Rüffer, M.N. Arshad, A.M. Asiri, Synthesis and structure characterization of Pt(IV) and Cd(II) 1,10-phenanthroline complexes; fluorescence, antitumor and photocatalytic property, J. Mol. Struct. 1192 (2019) 230-240.

[51] S.E.H. Etaiw, T.A. Fayed, M.M. El-bendary, H. Marie, Three ⅋ imensional coordination polymers based on trimethyltin cation with nicotinic and isonicotinic acids as anticancer agents, Appl. Organomet. Chem. 32 (2018) e4066.

[52] M.M. El-Bendary, E.D.H. Etaiw, Structure and applications of organotin complex based on trimethyltin cation and quinaldic acid: Structure and applications of organotin quinaldic acid complex, Appl. Organomet. Chem. 32 (2017) e4152.

[53] E.D.H. Etaiw, A.S. Sultan, M.M. El-Bendary, In vitro and in vivo antitumor activity of novel 3D-organotin supramolecular coordination polymers based on CuCN and pyridine bases, J. Organomet. Chem. 696(8) (2011) 1668-1676.

[54] E.D.H. Etaiw, M.M. El-Bendary, A new organometallic complex based on the trimethyltin cation and 2,6-pyridinedicarboxylic acid as a potential anticancer agent, Polyhedron 87 (2015) 383-389.

[55] L.R. Sherman, F. Huber, Relationship of cytotoxic groups in organotin molecules and the effectiveness of the compounds against leukemia, Appl. Organomet. Chem. 2 (1988) 65-72.

[56] M.A. Girasolo, A. Attanzio, P. Sabatino, L. Tesoriere, S. Rubino, G. Stocco, Organotin(IV) derivatives with 5,7-disubstituted-1,2,4-triazolo[1,5-a]pyrimidine and their cytotoxic activities: The importance of being conformers, Inorg. Chim. Acta 423 (2014) 168-176.

[57] H.-Y. Zhou, F.-Q. Dong, X.-L. Du, Z.-K. Zhou, H.-R. Huo, W.-H. Wang, H.-D. Zhan, Y.-F. Dai, M. Jing, Y.-P. Sui, J. Li, F. Sui, Y.-H. Zhai, Antitumor activities of biscoumarin and dihydropyran derivatives, Bioorg. Med. Chem. Lett 26 (2016) 3876-3880.

[58] Q.-P. Qin, S.-L. Wang, M.-X. Tan, Y.-C. Liu, T. Meng, B.-Q. Zou, H. Liang, Synthesis of two platinum(II) complexes with 2-methyl-8-quinolinol derivatives as ligands and study of their antitumor activities, Eur. J. Med. Chem. 161 (2019) 334-342.

[59] Q.-P. Qin, T. Meng, Z.-Z. Wei, C.-H. Zhang, Y.-C. Liu, H. Liang, Z.-F. Chen, Synthesis, Crystal Structure, Cytotoxicity, and Mechanism of Action of ZnII, MnII, and FeIII Complexes with 6-Hydroxyloxoisoaporphine, Eur. J. Inorg. Chem. 2017 (2017) 1824-1834.

[60] D. Wang, S.J. Lippard, Cellular processing of platinum anticancer drugs, Nature Reviews Drug Discovery 4 (2005) 307.

[61] T.C. Johnstone, K. Suntharalingam, S.J. Lippard, The Next Generation of Platinum Drugs: Targeted Pt(II) Agents, Nanoparticle Delivery, and Pt(IV) Prodrugs, Chem. Rev. 116 (2016) 3436-3486.

[62] K. Liu, H. Yan, G. Chang, Z. Li, M. Niu, M. Hong, Organotin(IV) complexes derived from hydrazone Schiff base: Synthesis, crystal structure, in vitro cytotoxicity and DNA/BSA interactions, Inorg. Chim. Acta 464 (2017) 137-146.

[63] G.-y. Yao, M.-y. Ye, R.-z. Huang, Y.-j. Li, Y.-m. Pan, Q. Xu, Z.-X. Liao, H.-s. Wang, Synthesis and antitumor activities of novel rhein α-aminophosphonates conjugates, Bioorg. Med. Chem. Lett 24 (2014) 501-507.

[64] C. Yan, J. Zhang, T. Liang, Q. Li, Diorganotin (IV) complexes with 4-nitro-N-phthaloyl-glycine: Synthesis, characterization, antitumor activity and DNA-binding studies, Biomed. Pharmacother. 71 (2015) 119-127.

[65] Y. Zhao, Z. Li, H. Li, S. Wang, M. Niu, Synthesis, crystal structure, DNA binding and in vitro cytotoxicity studies of Zn(II) complexes derived from amino-alcohol Schiff-bases, Inorg. Chim. Acta 482 (2018) 136-143.

[66] N. Ganji, A. Rambabu, N. Vamsikrishna, S. Daravath, Shivaraj, Copper(II) complexes with isoxazole Schiff bases: Synthesis, spectroscopic investigation, DNA binding and nuclease activities, antioxidant and antimicrobial studies, J. Mol. Struct. 1173 (2018) 173-182.

[67] I.M. El-Deen, A.F. Shoair, M.A. El-Bindary, Synthesis, structural characterization, molecular docking and DNA binding studies of copper complexes, J. Mol. Liq. 249 (2018) 533-545.

[68] Z. Mirzaei-Kalar, In vitro binding interaction of atorvastatin with calf thymus DNA: multispectroscopic, gel electrophoresis and molecular docking studies, J. Pharmaceut. Biomed. 161 (2018) 101-109.

Graphical abstract

Diversity of complexes based on p-nitrobenzoylhydrazide, benzoylformic acid and diorganotin halides or oxides self-assemble: cytotoxicity, the induction of apoptosis in cancer cells and DNA-binding properties

Wujiu Jiang[a, *], Shanji Fan,[b] Qian Zhou,[c] Fuxing Zhang,[a] Daizhi Kuang[a] and Yuxing Tan[a, *]

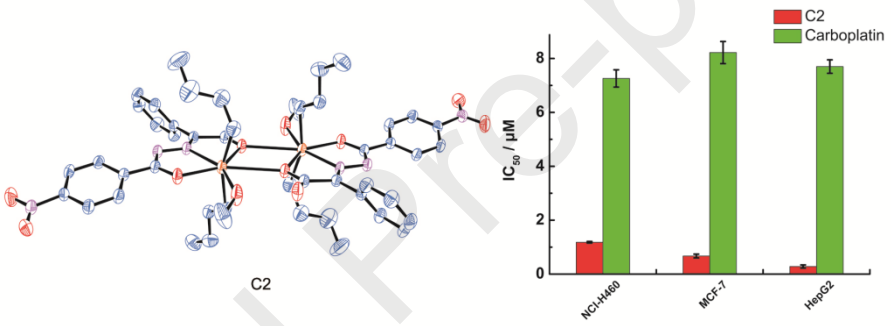

Eight organotin complexes have successfully prepared. In vitro antitumor activities test, **C2** has high activity and selectivity for inhibiting cancer cells.

Highlights

Eight organotin complexes were synthesized and characterized, and there exhibit four structural types.

Dibutyltin complex **C2** has high activity and selectivity for inhibiting cancer cells.

C2 is easy to synthesize, and may be developed as a new chemotherapeutic drug due to its excellent antitumor activity.

Declaration of interests

■ The authors declare that they have no known competing financial interests or personal relationships that could have appeared to influence the work reported in this paper.

☐The authors declare the following financial interests/personal relationships which may be considered as potential competing interests: